GEN-FOAM MODEL AND BENCHMARK OF DELAYED NEUTRON PRECURSOR DRIFT IN THE MOLTEN SALT REACTOR EXPERIMENT

Jun Shi and Massimiliano Fratoni

University of California, Berkeley
Department of Nuclear Engineering, Berkeley, CA 94720, USA

junshi@berkeley.edu, maxfratoni@berkeley.edu

ABSTRACT

The effective delayed neutron fraction is an important reactor kinetics parameter. In flowing liquid-fuel reactors, this differs from the delayed neutron fraction because of the emission of delayed neutrons with a lower energy spectrum than prompt and the delayed neutron precursor (DNP) drift due to the fuel movement. In general, neglecting delayed neutron precursor drift leads to an over-estimation of the effective delayed neutron fraction. Nevertheless, the capability to simulate this peculiar phenomenon is not available in most reactor physics tools. In this project, a multi-physics approach to modeling DNP drift is developed using the GeN-Foam toolkit, and it benchmarked against available experimental data from the Molten Salt Reactor Experiment (MSRE). GeN-Foam couples a neutron diffusion solver with a thermal-hydraulics solver. Additionally, a new function was added for solving adjoint multi-group diffusion eigenvalue problems and calculating effective delayed neutron fraction. For benchmarking, an R-Z model of the MSRE was developed in GeN-Foam. The porous media model was applied, and cross sections were generated using the Monte Carlo code Serpent-2 with ENDF/B-VII.1 nuclear data library. In order to evaluate the impact of DNP drift, two steady-state conditions (stationary and flowing salt at 1200 gpm) were simulated. A reactivity change of -241 pcm was calculated using GeN-Foam for the MSRE between static and flowing fuel, which is in a good agreement with the experimental value of -212 pcm. The total effective delayed neutron fraction change was calculated to be -230 pcm vs. -304 pcm reported for the MSRE and analytical calculated during the experimental campaign. Three transient accidents were also analyzed.

KEYWORDS: GeN-Foam, Delayed Neutron Precursor Drift, Effective Delayed Neutron Fraction, Molten Salt Reactor Experiment (MSRE)

1. INTRODUCTION

Molten Salt Reactors (MSRs) are designed to be fail-safe and can provide a path towards clean and sustainable nuclear energy, and after decades of discontinuance, a renewed interest in this Generation IV reactor technology is observed. The modeling of delayed neutron precursor (DNP) circulation in liquid fuel MSRs is identified as one of the particular phenomena that are not available in traditional reactor physics tools. In order to address this need, we will use and further develop a toolset that couples C++ multi-physics toolkit GeN-Foam [1] and the Monte Carlo code Serpent-2 [2].

The effective delayed neutron fraction (β_{eff}) is an important reactor kinetics parameter. The contribution of delayed neutrons is of primary importance for the safe control of any nuclear reactor. In circulating-fuel reactors (e.g., molten salt reactors), the effective delayed neutron fraction differs from the delayed neutron fraction (β_0) because of two distinct reasons. The first reason (common to solid-fuel reactors) is that the emission spectrum of delayed neutrons is softer than the of prompt neutrons: on average, the former are emitted with a lower energy. This may imply a difference in the importance of delayed and prompt neutrons. The second is that DNPs are transported by the fluid flow in the fuel circuit and may decay in positions of low importance and even out of the core. Spatial effects due to fuel motion are more relevant and always reduce the values of β_{eff}. Energy effects are, in general, of less relevance and may reduce or increase the effective delayed neutron fraction, according to the neutronic characteristics of the core. Therefore, the movement of DNPs complicates the calculation of the effective delayed neutron fraction and the accurate modeling of reactor transient responses.

This paper summarizes the modeling of Molten Salt Reactor Experiment in a 2 dimensional-RZ (2D-RZ) geometry in GeN-Foam, with cross sections generated by Serpent-2 and ENDF/B-VII.1 nuclear data library. Two steady-state calculations (static and fuel flowing at 1200 gpm) are performed, and the obtained results are analyzed and compared with data from Oak Ridge National Laboratory (ORNL) MSRE reports [3-4]. Three transient behaviors (unprotected transient over power, unprotected loss of heat sink, and unprotected loss of flow) are also discussed, respectively.

2. CALCULATION METHODOLOGY

The GeN-Foam multi-physics solver is built upon four main components: a thermal-hydraulics sub-solver, a neutronics sub-solver, a thermal-mechanics sub-solver, and a sub-scale fuel sub-solver. In our current study, only the first two sub-solvers are used. Thus, the calculation methodologies of neutronics and thermal-hydraulics sub-solvers are very briefly presented here, and a more detailed explanation of GeN-Foam code can be found in paper [1]. Note that all parameters are defined in section Nomenclature.

2.1. Thermal-hydraulics Sub-solver

The thermal-hydraulics sub-solver is based on the standard k-ε turbulence model for compressible or incompressible flows but extended to coarse-mesh applications through the use of a porous medium approach for user-selected cell zones inside the mesh. In other words, fine mesh can be applied for simple structures (e.g., plenum region), and coarse mesh can be applied for complex structures (e.g., core region and heat exchanger) by treating them as porous media. The equations for the turbulent single-phase flow of a fluid in a porous medium can be derived from standard Navier-Stokes (NS) equations, which govern the motion of fluids and can be seen as Newton's second law of motion for fluids, via time and volume averages. The resulting equations of mass, momentum and energy conservation are [5-7]:

$$\frac{\partial \gamma \rho}{\partial t} + \nabla \cdot (\rho \boldsymbol{u_D}) = 0 \,, \tag{1}$$

$$\frac{\partial \rho \boldsymbol{u_D}}{\partial t} + \frac{1}{\gamma}\nabla \cdot (\rho \boldsymbol{u_D} \otimes \boldsymbol{u_D}) = \nabla \cdot (\mu_T \nabla \boldsymbol{u_D}) - \gamma \nabla p + \gamma \boldsymbol{F_g} + \gamma \boldsymbol{F_{ss}} - (\rho \boldsymbol{u_D} \otimes \boldsymbol{u_D}) \nabla \frac{1}{\gamma} \,, \tag{2}$$

$$\frac{\partial \gamma \rho e}{\partial t} + \nabla \cdot \big(\boldsymbol{u_D}(\rho e + p)\big) = \gamma \nabla \cdot (k_T \nabla T) + \boldsymbol{F_{ss}} \cdot \boldsymbol{u_D} + \gamma \dot{Q}_{ss} + (k_T \nabla T) \cdot \nabla \gamma \,, \tag{3}$$

The appearance of a porosity γ considers the fact that only part of the volume is occupied by the fluid, and two additional terms, $\mathbf{F}_{SS}$ and $\dot{Q}_{ss}$, represent the effects on fluid flow by the sub-scale structures. In case of clear fluid, by setting porosity to 1 and sub-scale structures' effects to 0, these equations are converted back to the traditional Reynolds-averaged Navier-Stokes (RANS) equations. Therefore, the same set of equations can be discretized and solved on the same mesh while treating different zones of the geometry with two

different approaches (detailed RANS for clear fluid zone or coarse mesh porous medium for complex structure zone).

2.2. Neutronics Sub-solver

The neutronics sub-solver solves multi-group diffusion Eq. (4) and delayed neutron precursor concentration Eq. (5), including a precursor transport term based on a velocity field **u** for the analysis of DNP drift in a liquid fueled reactor (e.g., Molten Salt Reactor):

$$\frac{1}{v_i}\frac{\partial \varphi_i}{\partial t} = \nabla \cdot D_i \nabla \varphi_i + \frac{(1-\beta_t)\chi_{p,i}}{k_{eff}} \sum_{i=1}^{I} \nu\Sigma_{f,i}\varphi_i - \Sigma_{r,i}\varphi_i + \chi_{d,i} \sum_{k=1}^{K} \lambda_k C_k + S_{s,i} \,, \tag{4}$$

$$\frac{\partial C_k}{\partial t} + \nabla \cdot (\boldsymbol{u_D} C_k) = \frac{\beta_k \sum_j \nu\Sigma_{f,j}\varphi_j}{k_{eff}} - \lambda_k C_k \,, \tag{5}$$

In order to calculate the effective delayed neutron fraction in MSRE, the solution of both forward and adjoint multi-group diffusion eigenvalue problems are needed. Since the current version of GeN-Foam only solves the forward neutron flux, a function of computing adjoint neutron flux, according to paper [8], has been implemented. The equations related to the adjoint eigenvalue problems are given in Eqs. (6) and (7):

$$\nabla \cdot D_i \nabla \varphi_i^* - \Sigma_{r,i}\varphi_i^* + \sum_{j\neq i} \Sigma_{s,i\to j}\varphi_j^* + \frac{1-\beta_t}{k_{eff}} \nu\Sigma_{f,i} \sum_{i'=1}^{I} \chi_{p,i'}\varphi_{i'}^* + \frac{1}{k_{eff}} \nu\Sigma_{f,i} \sum_{k=1}^{K} \beta_k C_k^* = 0, \tag{6}$$

$$-\nabla \cdot (-\boldsymbol{u_D} C_k^*) + \nabla \cdot \frac{\nu_T}{Sc_T} \nabla C_k^* - \lambda_k C_k^* + \lambda_k \sum_{i=1}^{I} \chi_{d,i}\varphi_i^* = 0 \,, \tag{7}$$

After obtaining the forward and adjoint neutron flux distribution, the effective delayed neutron fraction for kth DNP group can be calculated as follows [8-9]:

$$\beta_{eff,k} = \frac{\int_{all\ space} \sum_{i=1}^{I} \varphi_i^* \chi_{d,i} \lambda_k C_k}{\int_{all\ space} \sum_{i=1}^{I} \varphi_i^* \chi_{d,i} \sum_{k'=1}^{K} \lambda_{k'} C_{k'} + \int_{all\ space} \sum_{i=1}^{I} \varphi_i^* \chi_{p,i} \sum_{i'=1}^{I} \varphi_{i'} \nu\Sigma_{f,i'}} \,, \tag{8}$$

Note that the value of cross sections, diffusion coefficients and neutron emission spectra are generated by Monte Carlo code Serpent-2, and the number and structure of both neutron energy and DNP groups are based on user's selection. For cross section parametrization in GeN-Foam, eight different perturbated states (i.e., nominal condition, increased/decreased fuel temperature, increased/decreased coolant density, increased/decreased coolant temperature, increased/decreased boron concentration, axially expanded fuel, radial expanded core, and expanded cladding) can be fed to the solver. Linear interpolation between nominal state and perturbed state is applied except the fuel temperature, for which the process can be based either on the logarithm or the square root of temperature, depending on fast or thermal neutron spectrum, respectively.

3. MOLTEN SALT REACTOR EXPERIMENT MODEL IN GEN-FOAM

The Molten Salt Reactor Experiment (MSRE) was built at the Oak Ridge National Laboratory and was operated from 1965 to 1969. Its purpose was to demonstrate key features of the molten salt fluid fuel concept and to prove the practicality of the MSR technology. This was the first large-scale, long-term, high-temperature testing performed for a fluid fuel salt, graphite moderator and new nickel-based alloys in a reactor environment. The circulating fuel was a mixture of lithium, beryllium, and zirconium fluoride salts that contained uranium fluorides. Reactor heat was transferred from the fuel salt to a similar coolant salt and was then dissipated to the atmosphere. The MSRE was designed to provide a thermal output of 10 MW [10].

3.1. 2D-RZ MSRE Geometry and Mesh in GeN-Foam

A 2D-RZ triangular mesh of MSRE, including the external loop, is generated by Gmsh [11] and shown in Fig. 1. The mesh is used for both thermal-hydraulics and neutronics solvers to simplify the calculations and eliminate possible errors when mapping fields between different meshes. The maximum mesh size is ~3 cm, with a refinement near the corners and peripheries by reducing it to ~3 mm. The model is divided into 11 regions, and the geometrical sizes of lower plenum, core, upper plenum and downcomer are consistent with MSRE design. However, it is difficult to model the external loop components (e.g., fuel pump, heat exchanger, etc.) in a 2D-RZ coordinate. Therefore, the external loop's geometry is artificial and determined based on the fuel salt volume from report ORNL-TM-728 [10]. The total fuel salt volume in the main stream is 67.3 ft^3 (1.906 m^3), and the volume in each region is listed in Table I. In GeN-Foam, the void (coolant) fraction is adjusted in order to match the fuel salt volume in MSRE design. By conserving fuel volume, fuel residence time can also be matched with MSRE design as long as the volumetric flow rate is same.

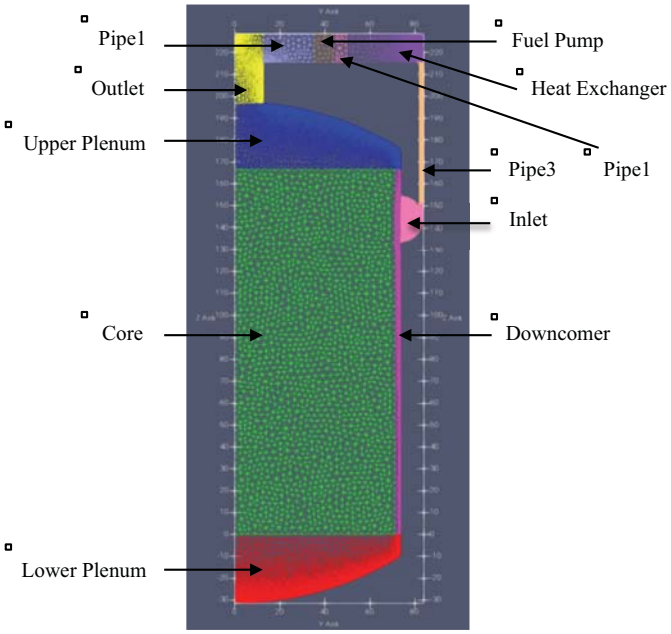

Figure 1. GeN-Foam 2D-RZ MSRE Thermal-hydraulics mesh [unit in cm].

Table I. MSRE Fuel Salt Volume and Residence Time [10].

Regions	Void Fraction in GeN-Foam	Fuel Salt Volume in GeN-Foam Model, m^3	Fuel Salt Volume in MSRE Design, m^3	Fuel Residence Time, s
Lower Plenum	79.08%	0.358 x 0.7908 = 0.283	0.283	3.8
Core	26.77%	2.645 x 0.2677 = 0.708	0.708	9.4
Upper Plenum	85%	0.350 x 0.85 = 0.297	0.297	3.9
Outlet	100%	0.016	0.059	0.8
Pipe1	100%	0.043		
Fuel Pump	100%	0.025	0.025	0.3
Pipe2	100%	0.023	0.023	0.3
Heat Exchanger	94.77%	0.182 x 0.9477 = 0.173	0.173	2.3
Pipe3	100%	0.062	0.062	0.8
Inlet	100%	0.082	0.275	3.6
Downcomer	100%	0.192		

3.2. Thermal-hydraulics Modeling

The MSRE core region, consisting of 1150 fuel channels and 618 graphite matrixes, is treated as a porous medium. A standard model is applied for coefficients of k-ε correlation [1], and Blasius correlation is used for Darcy friction coefficients [12]. The fuel pump is simulated by a momentum force in the direction of flow and able to establish a constant volumetric flow rate of 1200 gpm (0.07571 m^3/s), which equals to the operational flow rate in MSRE. In the heat exchanger zone, Darcy friction factors are adjusted to cause a pressure drop of ~140 kPa at nominal condition. The heat transfer with the secondary loop is simulated by a heat sink proportional to the temperature difference between primary loop and an external fluid at a fixed temperature of 845 K.

In the present work, the fuel salt is assumed to be incompressible, and its thermal-physical properties at 922 K are given in Table II. Some other assumptions include no control rods modeling, no heat transfer between core and downcomer, no bypass flow from downcomer to upper plenum, and a slip boundary condition for velocity variable on the wall. Besides, during our simulations, a few vortexes are observed when flow enters core from lower plenum. In order to eliminate them, a large flow resistance in the XY plane at the bottom of core is applied. This should not affect our steady-state results as long as the flow rate keeps at 1200 gpm. In reality, these vortexes are avoided by the existing of anti-swirl vanes in the lower plenum.

Table II. Fuel Salt Thermal-physical Properties at 922 K [13].

Parameters	Values
Density, kg m^{-3}	2258.6
Specific Heat, J kg^{-1} K^{-1}	1967.796
Dynamic Viscosity, Pa s	0.00785
Prandtl Number	10.7

3.3. Neutronics Modeling

According to the zero-power physics experiments on the MSRE [3], fuel salt composition at the time of criticality is 62.5LiF-31.6BeF_2-5.1ZrF_4-0.8UF_4 (expressed as molar percentages), and the mass fraction of ^{235}U in the salt is (1.408 ± 0.007) wt.%. Five different sets of homogenized cross sections (lower head, core, upper head, outlet pipe, and downcomer) are generated by Serpent-2 at 911 K and 1200 K as a reference state and a perturbated state, respectively, adopting ENDF/B-VII.1 nuclear data library with pre-defined energy group structures (default 2-group and CASMO 23-group) and six delayed neutron precursor groups (Table III). Their corresponding zones in GeN-Foam model are summarized in Table IV. In addition, two different types of boundary conditions are applied in GeN-Foam neutronics sub-solver. Zero-neutron-flux boundary condition is used for solving forward and adjoint neutron fluxes, and a reflective boundary condition is used for solving concentration and importance of DNPs.

Table III. DNP Groups Decay Constants from Serpent-2 Calculation Using ENDF/B-VII.1.

DNP groups	1	2	3	4	5	6
Decay Constant, s^{-1}	1.3336E-02	3.2737E-02	1.2079E-01	3.0283E-01	8.4972E-01	2.8537E+00

Table IV. Serpent-2 Cross Sections with their Corresponding Regions in GeN-Foam.

Serpent Cross Sections	Corresponding Regions in GeN-Foam Model
Lower Head	Lower Plenum
Core	Core
Upper Head	Upper Plenum
Outlet Pipe	Outlet, Pipe1, Fuel Pump, Pipe2, Heat Exchanger, and Pipe3
Downcomer	Inlet, Downcomer

4. RESULTS AND DISCUSSIONS

Two steady-state conditions (static and a constant flow rate of 1200 gpm) and three transient behaviors (unprotected transient over power, unprotected loss of heat sink, and unprotected loss of flow) are simulated and discussed in the following sections.

4.1. Steady-State Conditions

At the nominal flow rate of 1200 gpm, the velocity distritbution is shown in Fig. 2. Also, the values of temperature and pressure at reactor inlet, reactor outlet, heat exchanger inlet and heat exchanger outlet are measured, and they have a good agreement with MSRE design.

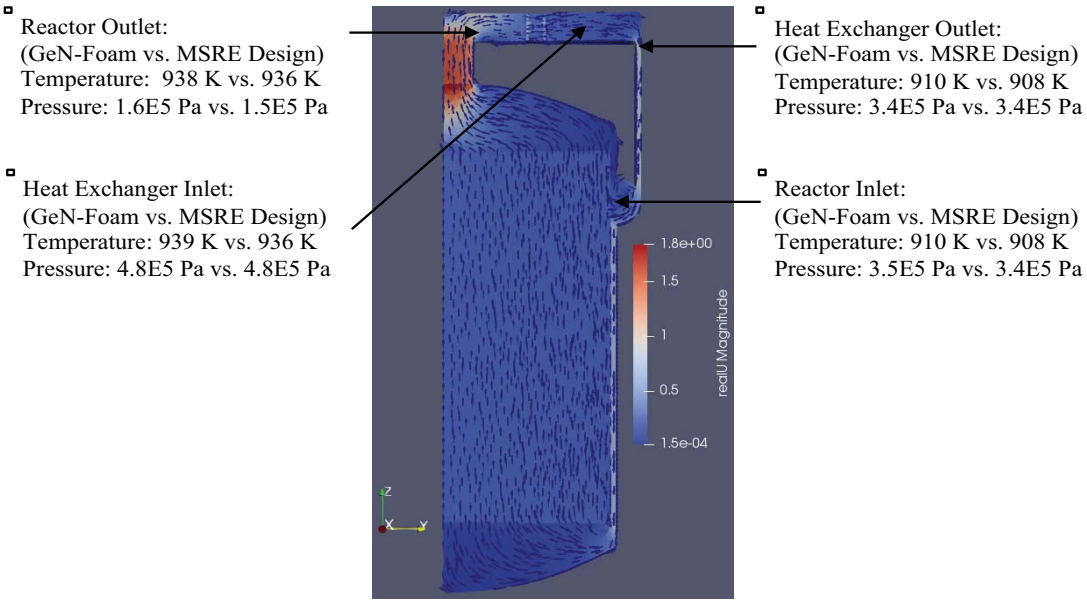

Figure 2. Velocity Profile at 1200 gpm.

4.1.1. Effective multiplication factor (k_{eff}) and effective delayed neutron fraction (β_{eff})

The k_{eff} and β_{eff} calculated by GeN-Foam are summarized in Table V and Table VI, respectively. The results from 2- and 23-energy group structures are very close, less than 25 pcm difference. However, some other numbers of group structures have also been used in calculations, and k_{eff} value does not converge until using 23-energy group structures. Therefore, a cancellation of errors occurs with 2-energy group structures.

Table V. k_{eff} Values from GeN-Foam.

Number of Energy Group	0 gpm	1200 gpm	Reactivity change ($\Delta\rho$)
Serpent Default 2	1.01232	1.00973	-0.00253
Serpent (CASMO 23)	1.01243	1.00996	-0.00241

Table VI. β_{eff} Values from GeN-Foam.

DNP groups	G1	G2	G3	G4	G5	G6	Total
Static condition (2-EG)	2.45E-04	1.22E-03	1.18E-03	2.62E-03	1.07E-03	4.61E-04	0.00680
Static condition (23-EG)	2.41E-04	1.20E-03	1.14E-03	2.59E-03	1.07E-03	4.68E-04	0.00671
1200 gpm (2-EG)	1.16E-04	5.09E-04	5.84E-04	1.80E-03	9.62E-04	4.54E-04	0.00443
1200 gpm (23-EG)	1.17E-04	5.13E-04	5.73E-04	1.79E-03	9.62E-04	4.61E-04	0.00441

As the fuel circulates, the k_{eff} value drops as expected, and the reactivity change of -241 pcm agrees with the data of -212 pcm from report ORNL-4233 [3]. The absolute value of total β_{eff} change of -230 pcm is smaller than that of -304 pcm from report ORNL-TM-380 [4]. The discrepancy is due to the simplification in ORNL's MSRE modelling, which the fission of delayed neutron is only considered in the graphite-moderated core region and the contribution of delayed neutrons emitted in the upper and lower plenum is not included. This leads to an underestimation of β_{eff} when fuel is flowing, and thus the change of β_{eff} is overestimated.

4.1.2. Delayed neutron precursor distribution (DNP group 1, 3, and 6 using 23-energy group)

The DNP concentrations at static and circulating conditions in MSRE are plotted from Figs. 3 to 5. Note that due to page limits, only DNP group 1, 3, and 6 are presented for demonstration.

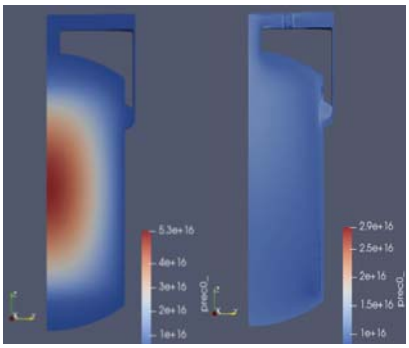

Figure 3. DNP_1 (static vs. flow).

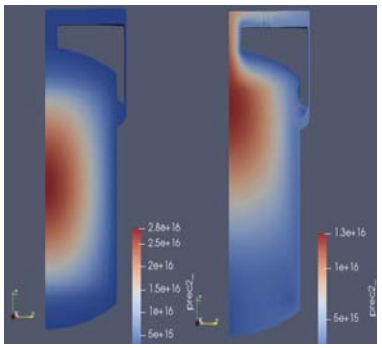

Figure 4. DNP_3 (static vs. flow).

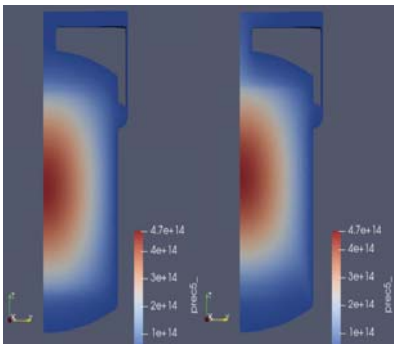

Figure 5. DNP_6 (static vs. flow).

For static fuel, the DNP concentrations have a similar shape as the total neutron flux since DNPs are not moving, and their concentrations are proportional to the neutron flux. When the fuel starts to circulate, significant changes can be observed from DNP_1 plots. This is because DNP drift as fuel moves, and DNP_1 has the smallest decay constant and longest half-life (greater than 50 s), so they have time to distribute all over MSRE core and external loop before decaying. As the decay constant increases and half-life decreases, DNP_3 has a higher concentration at the top of core and upper plenum region. Finally, for DNP_6 with the largest decay constant and shortest half-life (less than 1 s), they quickly decay before moving out of the core, resulting in minor changes on the DNP concentration plots.

4.2. Accident Transients

In most reactors, there are three main transient initiators, i.e., reactivity insertion, heat exchanger, and primary pump. The following subsections discuss the three possible MSRE responses to the corresponding transient initiators. Note that the main purpose of these analyses is to demonstrate the transient modeling capability of GeN-Foam because a few bugs have been identified and fixed during our study. In addition, even though the steady-state results agree with MSRE design and experimental data, the aforementioned assumptions in section 3.2 and the 2D-RZ geometry may affect the thermal-hydraulics calculations under various transient conditions. Thus, further investigations in this area are required.

4.2.1. Unprotected transient over power (UTOP)

An UTOP may occur following a reactivity insertion, which is particularly demanding from a numerical point of view, thus representing a good test for the models. It also gives rise to the maximum power excursion for a given reactivity insertion. For simplicity, three stepwise reactivity insertions have been investigated: 100 pcm (prompt subcritical), 440 pcm (prompt critical), and 500 pcm (prompt supercritical) reactivity insertions. In GeN-Foam, such reactivity insertions are introduced by directly changing k_{eff} values

at the beginning of transient calculations, and the resulting power and average fuel temperature profiles are given in Figs. 6 and 7, respectively.

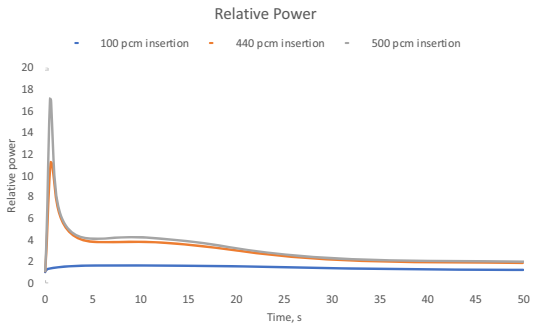

Figure 6. Relative Power in UTOP.

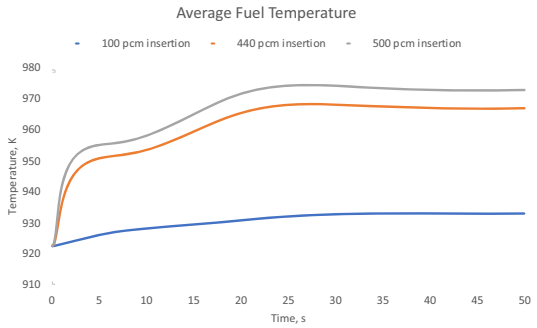

Figure 7. Average Fuel Temperature in UTOP.

It can be observed that by inserting a larger reactivity, a larger power peak occurs at an earlier time. The prompt power increase is triggered by a stepwise reactivity insertion and leads to a rapid temperature increase. Even the reactor is at the prompt critical ($\rho = \beta_{eff} = 0.44\%$) and prompt supercritical ($\rho = 0.5\% > \beta_{eff} = 0.44\%$) states, the consequent negative reactivity insertion due to Doppler effect is able to quickly reduces the power, and the final temperature increase is determined by the amount of initial reactivity inserted.

4.2.2. Unprotected loss of heat sink (ULOHS)

An ULOHS may occur following a loss of coolant salt in the reactor secondary loop. For simplicity, the loss of cooling capabilities of heat exchanger is simulated by removing all related heat transfer coefficients in the heat exchanger zone, and the resulting responses are shown in Figs. 8 and 9, respectively.

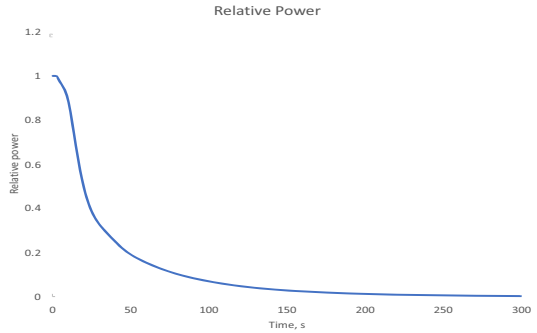

Figure 8. Relative Power in ULOHS.

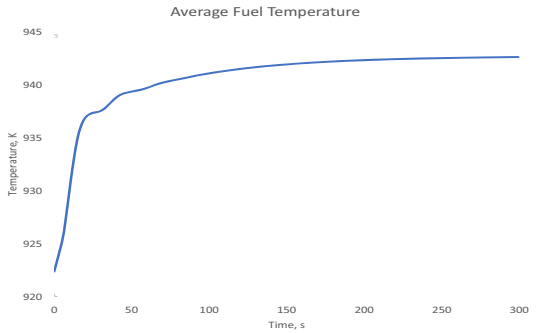

Figure 9. Average Fuel Temperature in ULOHS.

As soon as the cooling capabilities are lost, the fuel salt temperature increases, and thus temperature feedbacks quickly reduce the power and shut down the reactor. The temperature in the primary loop are gradually homogenized because the heat sink is completely removed. In fact, a more realistic scenario would include the effect of decay heat, which will further increase the fuel temperature and lead to a faster and larger power drop.

4.2.3. Unprotected loss of flow (ULOF)

An ULOF with a fuel pump coast-down may occur in a reactor following an electricity shortage. In this simulation, the pump force in the primary circuit is assumed to drop exponentially, starting from 1 second with a time constant of ~8 seconds. After ~27 seconds, the flow rate drops to 1/10 of the nominal operation

flow rate in Fig. 10, and the resulting power and average fuel temperature are plotted in Figs. 11 and 12, respectively.

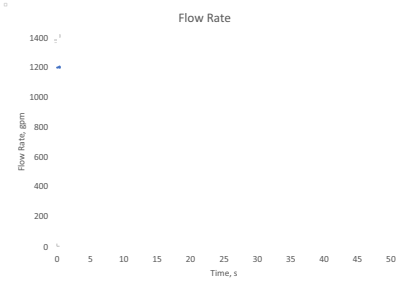

Figure 10. Flow Rate.

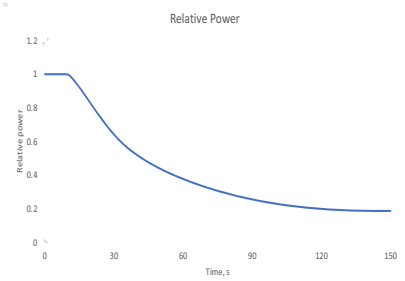

Figure 11. Relative Power.

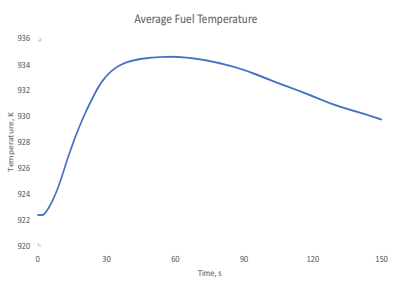

Figure 12. Avg. Fuel Temperature.

As the flow rate decreases, the heat removing capability is reduced and the average fuel temperature initially increases. This temperature increase introduces a negative reactivity due to the Doppler effect and thus reduces power. In fact, at the very beginning of transient (1 second to ~10 seconds), the power does not drop immediately because the speed of DNPs flowing out of the core becomes slower, resulting in a positive reactivity insertion and a minor power rise (not obvious in Fig. 11 due to the plot scale). Finally, the fuel temperature starts to decrease after reaching its peak point when the heat generating rate balances with the heat removing rate.

5. CONCLUSIONS

In order to benchmark the delayed neutron precursor drift in MSRE, a 2D-RZ multi-physics model is built in GeN-Foam by conserving the fuel volume and fuel residence time as MSRE design. The cross sections used in GeN-Foam are generated by the Monte Carlo code Serpent-2, adopting ENDF/B-VII.1 nuclear data at reference and perturbated temperatures of 911 K and 1200K, respectively. Serpent default 2- and CASMO 23-energy group structures are selected and compared in multi-group neutron diffusion calculations. Although the results are very close, two-energy group structures is not sufficient. For delayed neutron precursor concentration calculations, six DNP groups are chosen. For steady-state calculations (static and fuel flowing at 1200 gpm) with 23-energy group structures, the k_{eff} values are determined to be ~1.01243 and ~1.00996, respectively. The reactivity change of -241 pcm due to fuel circulation is close to MSRE report data of -212 pcm. An adjoint neutron flux solver is also developed and implemented in GeN-Foam to evaluate the effective delayed neutron fractions. The $\beta_{eff,\,total}$ is calculated as 0.671% without DNP drift and 0.441% with DNP drift, respectively. The absolute value of $\Delta\beta_{eff,\,total}$ of -230 pcm is smaller than the estimated change of -304 pcm from MSRE report. This discrepancy is due to the omitting of contribution to fission of delayed neutrons emitted in the upper and lower plenum. Moreover, velocity, temperature, pressure, and delayed neutron precursor concentration have been analyzed and shown a reasonable agreement with data from the MSRE. Furthermore, three possible accidental transients (UTOP, ULOHS, and ULOF) have been simulated and discussed. Future improvements may consider modeling of control rods and bypass flow from downcomer to upper plenum region, mesh refinement near walls, and upgrading the model from 2-D to 3-D.

NOMENCLATURE

C_k concentration for k^{th} DNP group, [m^{-3}]
C_k^* importance of the k^{th} delayed neutron precursor group, [m^{-2} s^{-1}]
D_i neutron diffusion coefficient for i^{th} energy group, [m]
e coolant total energy, [J kg^{-1}]
$\mathbf{F_g}$ volumetric force due to gravity, [N m^{-3}]

$\mathbf{F_{ss}}$ volumetric force due to the interaction with the sub-scale structure, [N m^{-3}]
k_{eff} effective multiplication factor, [-]
k_T turbulent conductivity, [W m^{-1} K^{-1}]
p pressure, [Pa]
$\dot{Q}_{ss}$ heat transferred from the sub-scale structure to the fluid, [W m^{-3}]
Sc_T turbulent Schmidt number, [-]
$S_{s,i}$ scattering neutron source from neutron energy groups others than $i^{th} = \sum_{j \neq i} \Sigma_{j \to i} \varphi_j$, [$m^{-3}$ s^{-1}]
u coolant velocity, [m s^{-1}]
$\mathbf{u_D}$ Darcy coolant velocity = $\gamma\mathbf{u}$, [m s^{-1}]
v_i average neutron velocity for i^{th} energy group, [m s^{-1}]
$\beta_{eff,\,k}$ effective delayed neutron fraction for k^{th} DNP group, [-]
$\beta_{eff,\,total}$ total effective delayed neutron fraction, [-]
γ porosity, [-]
μ_T turbulent dynamic viscosity, [Pa s]
λ_k decay constant for k^{th} DNP group, [s^{-1}]
ν average number of neutrons per fission, [-]
ν_T turbulent kinematic viscosity, [m^2 s^{-1}]
ρ coolant density, [kg m^{-3}]
$\Sigma_{f,i}$ fission cross section of i^{th} energy group, [m^{-1}]
$\Sigma_{j \to i}$ group-transfer cross section from j^{th} to i^{th} energy group, [m^{-1}]
$\Sigma_{r,i}$ removal cross section for i^{th} energy group, [m^{-1}]
φ_i neutron flux for i^{th} energy group, [m^{-2} s^{-1}]
φ_i^* adjoint neutron flux for the i^{th} energy group, [m^{-2} s^{-1}]
$\chi_{d,i}$ delayed neutron yield for i^{th} energy group, [-]
$\chi_{p,i}$ prompt neutron yield for i^{th} energy group, [-]

REFERENCES

1. C. Fiorina, I. Clifford, M. Aufiero, and K. Mikityuk, "GeN-Foam: A Novel OpenFOAM based Multi-physics Solver for 2D/3D Transient Analysis of Nuclear Reactors," *Nuclear Engineering and Design* **294**, pp. 24-37 (2015).
2. J. Leppänen, et al., "The Serpent Monte Carlo Code: Status, Development and Applications in 2013," *Ann. Nucl. Energy* **82**, pp. 142-150 (2015).
3. B.E. Prince, S.J. Ball, J.R. Engel, P.N. Haubenreich, and T.W. Kerlin, *Zero-power Physics Experiments on the Molten-salt Reactor Experiment*, Oak Ridge National Laboratory, Oak Ridge, Tennessee, USA (1968).
4. P.N. Haubenreich, *Prediction of Effective Yields of Delayed Neutrons in MSRE*, Oak Ridge National Laboratory, Oak Ridge, Tennessee, USA (1962).
5. I. Clifford, *A Hybrid Coarse and Fine Mesh Solution Method for Prismatic High Temperature Gas-cooled Reactor Thermal-fluid Analysis*, Penn State University, State College, Pennsylvania, USA (2013).
6. R. Saurel, and R. Abgrall, "A Multiphase Godunov Method for Compressible Multifluid and Multiphase Flows," *Journal of Computational Physics* **150**(2), pp. 425-467 (1999).
7. K. Vafai, *Handbook of Porous Media*, CRC Press, New York, USA (2005).
8. M. Aufiero, et al., "Calculating the Effective Delayed Neutron Fraction in the Molten Salt Fast Reator: Analytical, Deterministic and Monte Carlo Approaches," *Annals of Nuclear Energy* **65**, pp. 78-90 (2014).
9. F. Mattioda, P. Ravetto, and G. Ritter, "Effective Delayed Neutron Fraction of Fluid-fuel Systems," *Annals of Nuclear Energy* **27**(16), pp. 1523-1532 (2000).

10. R.C. Robertson, *MSRE Design and Operations Report Part I Description of Reactor Design*, Oak Ridge National Laboratory, Oak Ridge, Tennessee, USA (1965).
11. C. Geuzaine, and J.F. Remacle, "Gmsh: A Three-Dimensional Finite Element Mesh Generator with Built-in Pre- and Post-processing Facilities," *International Journal for Numerical Methods in Engineering* **79**(11), pp. 1309-1331 (2009).
12. J. Bao, *Development of the Model for the Multi-physics Analysis of Molten Salt Reactor Experiment using GeN-Foam Code.* Paul Scherrer Institute, Villigen, Switzerland (2016).
13. R.J. Kedl, *Fluid Dynamic Studies of the Molten-Salt Reactor Experiment (MSRE) Core*, Oak Ridge National Laboratory, Oak Ridge, Tennessee, USA (1970).